Spin and spatial dynamics in electron-impact scattering off *S*-wave He using *R*-matrix-with-time-dependence theory

Jack Wragg and Hugo W. van der Hart
Centre for Theoretical Atomic, Molecular and Optical Physics, School of Mathematics and Physics, Queen's University Belfast, Belfast BT7 1NN, United Kingdom

(Received 10 May 2016; published 13 September 2016)

R-matrix-with-time-dependence theory is applied to electron-impact ionization processes for He in the *S*-wave model. Cross sections for electron-impact excitation, ionization, and ionization with excitation processes for impact energies between 25 and 225 eV are in excellent agreement with benchmark cross sections. Ultrafast dynamics induced by a scattering event is observed through time-dependent signatures associated with autoionization from doubly excited states. Further insight into dynamics can be obtained through examination of the spin components of the time-dependent wave function.

DOI: 10.1103/PhysRevA.94.032706

I. INTRODUCTION

Scientific progress greatly benefits from the development of theoretical and computational methods that complement new experimental techniques. Recent developments in the study of electron dynamics on the sub-femtosecond timescale [1–4] have enhanced the need for the development of computational models able to obtain a time-dependent description of ultrafast multielectron processes. In the present paper, we demonstrate a time-dependent *ab initio* computational method for the study of electron spatial and spin dynamics through its application to electron-He impact processes in the *S*-wave model (known as the Temkin-Poet model when applied to electron-hydrogen scattering [5,6]). We choose this particular model as it provides a simple atomic process which contains both spin and spatial dynamics, and for which benchmark data for comparison is readily available [7,8].

Electron-impact processes for He in the *S*-wave model were investigated through application of the time-dependent Close-Coupling (TDCC) approach [9]. Since then, a range of other advanced approaches have been applied to investigate this problem, including the convergent close-coupling approach [10–12] and the exterior-complex-scaling approach (ECS) [7,8,13]. We note that this description of a three-electron system bears great similarity to the time-dependent calculation of Li processes in [14], since the restriction in angular momentum corresponds to a 1D description for each electron.

In this paper, we build upon the *R*-matrix with time-dependence (RMT) theory [15,16]. This approach combines the *R*-matrix division of configuration space with time propagation to model attosecond processes in many-electron atoms. RMT has recently provided valuable insights into high-harmonic generation [17], and experimental attosecond transient absorption spectroscopy data [18]. The RMT approach has been extended to model dynamics in atomic systems where two electrons are ejected from the core, demonstrated with an application to double photoionisation from a Helium atom [19].

We use RMT theory to consider ultrafast dynamics that occur within electron-impact excitation, ionization, and in particular ionization-excitation processes. Whereas previous application of RMT theory for two electron ejection considered systems with a single double-ejection threshold, the present study investigated the numerical accuracy of the approach for systems with multiple thresholds. The present process provides an opportunity to robustly assess the numerical techniques in the RMT approach through quantitative comparison with present data for electron-impact of He in the *S*-wave model [7,8,11–13].

The treatment of this particular problem provides a stepping stone towards the development of an RMT approach for the full treatment of double ionization in general atomic systems. The backbone of the treatment would be formed by states consisting of a double ionization threshold of two or more free electrons. The electron-He scattering process can be regarded as the simplest of such systems. The RMT approach for this scattering process thus offers a clear development path towards a general atomic code for the treatment of double ionization. In addition to this, the time-dependent nature of the RMT treatment can provide dynamical insight into the scattering processes. For example, whereas the excitation of autoionizing states in this scattering process has been considered previously [13], a time-dependent treatment can reveal clear signatures of dynamics within these states. Furthermore, a time-dependent method, such as RMT also allows the spin coupling between the electrons to be traced during the scattering process.

Throughout this paper, we use atomic units unless otherwise stated.

II. THEORY

In RMT, the three-electron *S*-wave Hamiltonian

$$\hat{H} = \sum_{n=1}^{3}\left(-\frac{1}{2}\frac{d^2}{dr_n^2} - \frac{2}{r_n}\right) + \frac{1}{r_{12}^{>}} + \frac{1}{r_{13}^{>}} + \frac{1}{r_{23}^{>}}, \qquad (1)$$

is used within the Schrödinger equation

$$i\frac{d}{dt}\Psi(\vec{R},\chi,t) = \hat{H}\Psi(\vec{R},\chi,t), \qquad (2)$$

where $\vec{R}$ is the position vector (r_1,r_2,r_3) and r_n is the radial coordinate of electron n. $r_{n'n''}^{>}$ is the greater of $r_{n'}$ and $r_{n''}$. $\Psi(\vec{R},\chi,t)$ is the time-dependent wave function, where χ indicates the spin coupling of the electrons.

Three regions of configuration space are defined within RMT for two-electron ejection [19]: region (I) with r_1,r_2,

$r_3 < b$, where b is the size of the so-called inner region; region (II), where $r_1, r_2 < b$ and $r_3 > b$; and region (III), where $r_1 < b$ and $r_2, r_3 > b$. The RMT wave function in each region is described in terms of a time-dependent coefficient and a time-independent basis as

$$\text{(I)}\quad \Psi(\vec{R},\chi,t) = \sum_j C_j^{(\mathrm{I})}(t)\psi_j^{(\mathrm{I})}(r_1,r_2,r_3,\chi), \tag{3}$$

$$\text{(II)}\quad \Psi(\vec{R},\chi,t) = \sum_k C_k^{(\mathrm{II})}(r_3,t)\psi_k^{(\mathrm{II})}(r_1,r_2,\chi), \tag{4}$$

$$\text{(III)}\quad \Psi(\vec{R},\chi,t) = \sum_m C_m^{(\mathrm{III})}(r_2,r_3,t)\psi_m^{(\mathrm{III})}(r_1,\chi), \tag{5}$$

where the coefficients $C_k^{(\mathrm{II})}(r_3,t)$ and $C_m^{(\mathrm{III})}(r_2,r_3,t)$ are defined at FD grid points across $r_3 > b$, and $r_2, r_3 > b$, respectively. k and m correspond to single- and two-electron channels in regions (II) and (III), respectively, whereas j indicates a region-(I) eigenstate. Three-electron escape corresponding to $r_1, r_2, r_3 > b$ is not considered. Configuration space not covered in regions (I), (II), and (III) is included via antisymmetrization of the wave function.

The basis functions $\psi^{(N)}$ are expanded in terms of a further basis of functions $\zeta_k^{(N)}$ [for (N) = (I), (II), and (III)] and appropriate spin functions. These $\zeta_k^{(N)}$ functions are, in turn, constructed from antisymmetrized products of hydrogenic eigenfunctions $\zeta_n^+(r_i)$, corresponding to the nth eigenvalue of the operator

$$\hat{H}_i^+ = -\frac{1}{2}\frac{d^2}{dr_i^2} - \frac{2}{r_i} + L_b, \tag{6}$$

where L_b is the Bloch operator [20], written as

$$L_b = \frac{1}{2}\delta(r_i - b)\frac{d}{dr_i}. \tag{7}$$

To minimize the number of basis functions, at least one of the electrons within the inner region ($r_i < b$) is restricted to the lowest three eigenstates. This "core" electron is thus restricted to the $1s$, $2s$, and $3s$ orbitals. We obtain eigenfunctions for the inner-region ($r_i < b$) aspect of the wave function in each of the three regions through diagonalization of the following Hamiltonians:

$$\begin{aligned}
&\text{(I)} \quad \hat{H}_1^+ + \hat{H}_2^+ + \hat{H}_3^+ + \frac{1}{r^>{}_{12}} + \frac{1}{r^>{}_{23}} + \frac{1}{r^>{}_{13}},\\
&\text{(II)} \quad \hat{H}_1^+ + \hat{H}_2^+ + \frac{1}{r^>{}_{12}},\\
&\text{(III)} \quad \hat{H}_1^+,
\end{aligned} \tag{8}$$

where $\hat{H}_i^+$ is the hydrogenic Hamiltonian given in Eq. (6).

As with previous RMT implementations, the wave function is propagated in time from an initial state at $t = t_0$. This initial state contains two electrons in the He ground state and an incoming s electron, described by a Gaussian wave packet with a rms width of $10a_0$ centered on $r_3 = 75a_0$.

In this study, we use a sixth-order Taylor-series propagator. The kinetic-energy operations on the coefficients defined across FD grids [$-\frac{1}{2}\frac{d^2}{dr_3^2}$ in region (II) and $-\frac{1}{2}\frac{d^2}{dr_2^2}, -\frac{1}{2}\frac{d^2}{dr_3^2}$ in region (III)] are evaluated using FD operators. Near the inner boundary of regions (II) and (III), the FD grids contain insufficient grid points to complete the center-difference FD operation. The missing data points are hence obtained from the wave function in region (I) or region (II), respectively. Additionally, propagation using the physical three-electron Hamiltonian in Eq. (1) requires cancellation of the Bloch operator terms contained within $\hat{H}_3^+$ [region (I)] and $\hat{H}_2^+$ [region (II)], as defined in Eq. (8). This is achieved through the evaluation of an FD first-derivative operation on the wave function at the boundary between regions (I) and (II), and the boundary between regions (II) and (III), as implemented in [19].

The initial wave function is propagated in time until the scattered electron has moved well away from the residual atom or ion. Electron-impact excitation yields are then obtained from the total population in the relevant region-(II) channel. Electron-impact ionization yields are obtained from the total population in region (III) associated with a particular residual He^+ state ($1s$, $2s$, or $3s$). These yields are then transformed into electron-impact scattering cross sections.

III. RESULTS

Figure 1 shows impact excitation and ionization cross sections for He in the S-wave model over the electron-impact energy range between 25 and 225 eV. For all processes shown, we observe good agreement with the benchmark data. The largest difference (25%) is seen at large impact energies for electron-impact ionization with excitation of the residual ion to the $2s$ state, where the restriction of the core electron to $1s$, $2s$, or $3s$ could have a more significant effect on the modeling. We also note a more pronounced difference near the threshold for electron-impact ionization. In this energy range, the main difficulty lies in distinguishing two-electron ejection from the excitation of high-lying excited states (a similar challenge was encountered in [19]). Overall, the cross sections for electron-impact scattering show excellent agreement with those obtained in [7] and demonstrate the accuracy of the present approach.

Following excitation, the population of the $2s2s$ state decreases over time as the state autoionizes. In Fig. 2, the population of the channel associated with the $2s2s$ state in region (II) is shown as the calculation propagates in time. We note that the sharp increase in yield (light red points) corresponds not to the excitation of the $2s2s$ state, but rather to the flow of the scattered electron in the $2s2s$ channel from region (I) into region (II). The exponential decay of the $2s2s$ state is then seen in Fig. 2 (dark red points). The light blue line is a fit of the exponential decay function $A\exp(-\gamma t)$ to the dark red points. From this fit, a $2s2s$ decay rate of $\gamma = 1.10 \times 10^{14}\ \mathrm{s}^{-1}$ is obtained, which agrees to within 10% with the decay rate given in [7]. The earliest dark red point is taken as the yield for the $2s2s$ state, from which the value for the $2s2s$ cross sections shown in Fig. 1 is calculated. The moment of collision in the calculation shown in Fig. 2 is estimated to happen approximately 1.1 fs after the beginning of the calculation, with the first reliable $2s2s$ yield obtained approximately 0.5 fs later. We estimate that this lack of access to an immediate $2s2s$ yield introduces an uncertainty of approximately 10% to the RMT $2s2s$ cross section.

Previous studies have shown the theoretical time-dependent description of autoionization to be an interesting challenge [21–23]. We can identify such autoionization dynamics

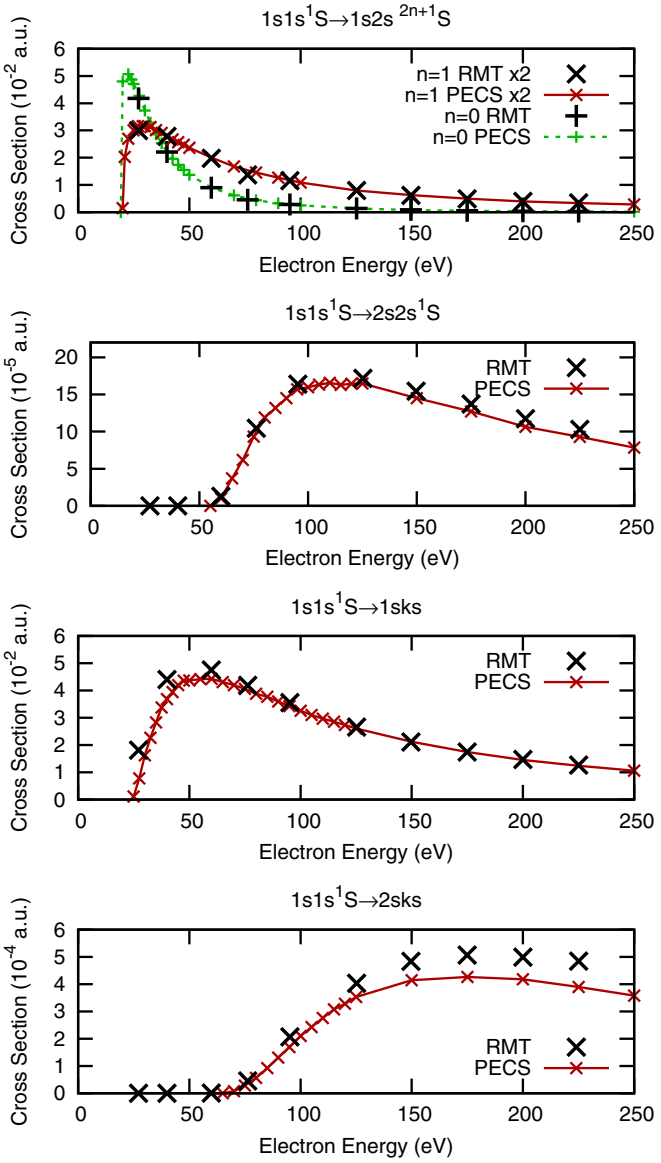

FIG. 1. Electron-impact cross sections for He in the S-wave model for impact energies between 25 and 225 eV as obtained in the RMT approach. Cross sections for electron-impact excitation to $1s2s$ and $2s2s$; electron-impact ionization, leaving He^+ in $1s$; and electron-impact ionization with excitation of He^+ to $2s$. All cross sections are compared with benchmark data (calculated using the PECS method) from [7,8].

within the RMT model of the scattering process. We show in Fig. 3 the probability density associated with a residual He^+ ion in the $1s$ state at 11.96 fs after the beginning of the model. The direct electron-impact-ionization wave packet can be seen as an arc from $\sqrt{r_2^2+r_3^2} \approx 750a_0$ to $\sqrt{r_2^2+r_3^2} \approx 1050a_0$. In addition to this arc, a series of six peaks is seen along along $r_3 \approx 535a_0$ and $r_2 \approx 535a_0$. These peaks signify dynamics associated with doubly excited $2sns$ states and their autoionization. The different natures of the two processes are reflected in the strong interference where this series and arc overlap. We consider that the distance along coordinate r_3 at time t corresponds to the momentum of a

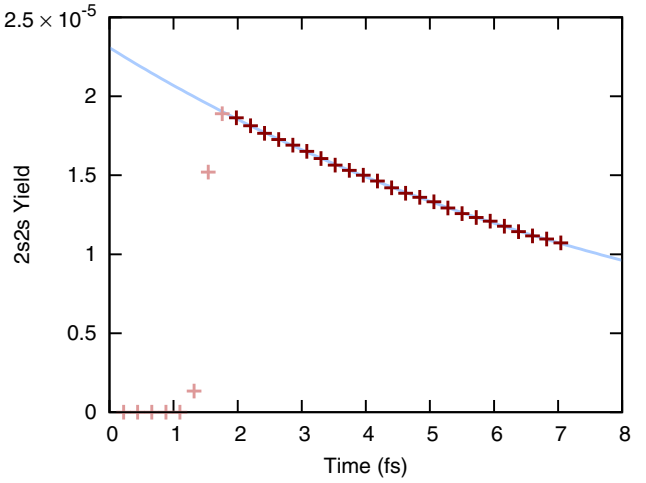

FIG. 2. Yield of the $2s2s$ state in region (II). Light red data points indicate a yield obtained before the excited wave packet has entered region (II), and dark red data points indicate a yield obtained after the wave packet has entered region (II). The blue line indicates an exponential decay fit of the dark red points.

scattered electron after excitation of a doubly excited $2sns$ state, i.e., $r_3 = (t - t_c)/k_{i_n}$. Here t_c is the value of t at the moment of collision, and k_{i_n} is the momentum of the impact electron after exciting the atom to the $2sns$ autoionizing state. Sometime after the moment of collision, the $2sns$ state autoionizes, leading to emission of an electron associated with the r_2 radial coordinate. Since this autoionized electron has a well-defined momentum, r_2 and t can be mapped to the moment of autoionization $\tau_n(r_2,t)$ from state $2sns$ as

$$\tau_n(r_2,t) = t - t_c - r_2/\sqrt{2E_n}, \tag{9}$$

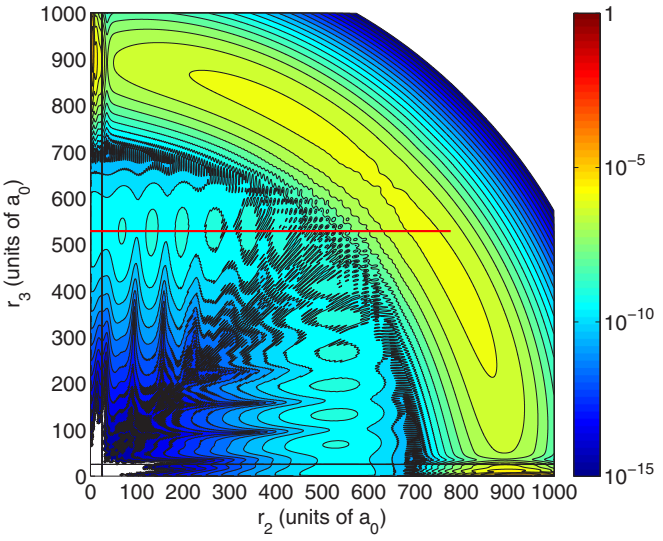

FIG. 3. Probability density of finding electrons 2 and 3 at positions r_2 and r_3 when the residual He^+ ion in the S-wave model is left in the $1s$ state. The density shown is obtained after 11.96 fs for an incoming electron wave packet of 76 eV, initially centered at $75a_0$. The red line at $r_3 = 535a_0$ indicates data shown in Fig. 4, associated with autoionization of the $2sns$ states.

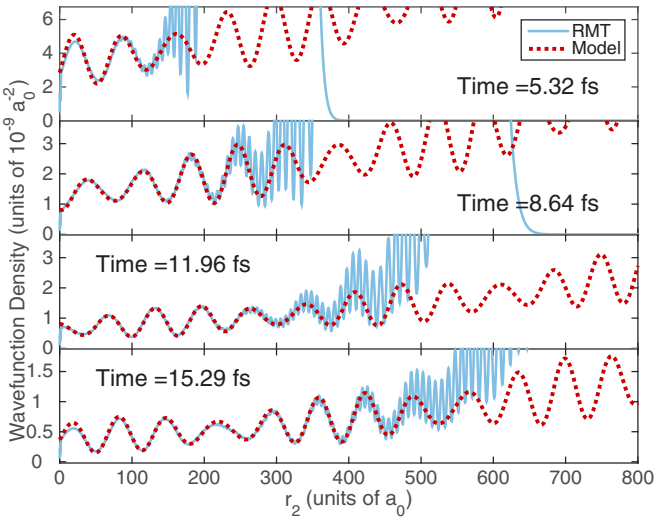

FIG. 4. Wave-function density along the lines $r_3 = 704a_0, 535a_0, 375a_0, 217a_0$ at times 15.29, 11.96, 8.64, and 5.32 fs after the start of the model, respectively. The 11.96-fs data correspond to the data shown in Fig. 3. The RMT density (blue) is compared to model data (red), obtained as described in the text. The variations in the density correspond to time variation in the autoionization rate of a superposition of $2sns$ states.

such that the autoionized electron has traveled from $r = 0$ at time of emission $\tau_n(r_2,t)$ to $r = r_2$ at time t. Interference between autoionization contributions from $2s2s$ and higher $2sns$ states then gives a time-dependent autoionization rate for the doubly excited He atom, which is reflected in the series of peaks in Fig. 3.

Figure 4 shows the probability density along the autoionization wave packet (as described by the red line in Fig. 3) at four moments during the calculation along with a model of the autoionization arising from the $2sns$ states. The wave packet along r_2 is modeled by considering the autoionization of the $2s2s$, $2s3s$, and $2s4s$ states:

$$P(r_2,t) = C\left|\sum_{n=2}^{4}\sqrt{\sigma_n\gamma_n e^{-\gamma_n\tau_n(r_2,t)}}\exp\left[i(k_n r_2 - E_n t)\right]\right|^2. \quad (10)$$

In these equations, E_n is the energy of the $2sns$ state, γ_n is its autoionization rate, and σ_n is its cross section. These quantities are obtained from [7]. It is possible to obtain initial estimates for the normalization constant C from the shape of the R-matrix wave packet. However, for the sake of avoiding unnecessary complication, we obtain C by a fit to each RMT data set. Figure 4 shows close agreement between the model and the RMT density. The rapid oscillations in Fig. 4 with a wavelength of $\approx 55a_0$ are related to interference between autoionization from $2s2s$ and from the superposition of $2s3s$ and $2s4s$. The modulation of these oscillations with a wavelength of $\approx 270a_0$ is associated with the interference between autoionization from $2s3s$ and $2s4s$. Hence the sequence of peaks follows the time-varying autoionization of the doubly excited residual He atom.

We now turn to a demonstration of the capability of the RMT approach to describe spin dynamics as well as spatial dynamics. We note that RMT does not currently directly solve

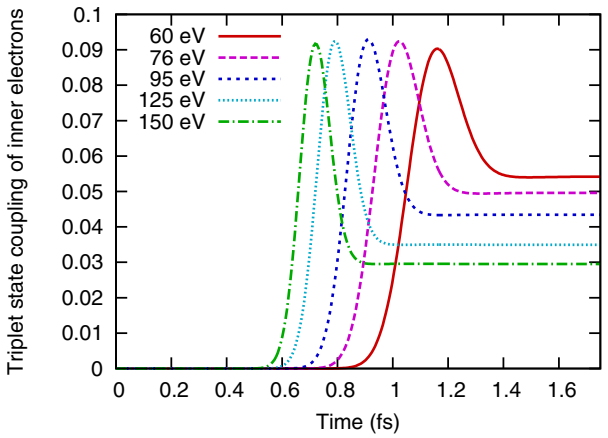

FIG. 5. The fraction of the wave function in which the two innermost electrons are coupled to a triplet state as a function of time for different impact energies in electron scattering off He in the S-wave model.

the relativistic Pauli or Dirac equations as the regimes of interest here are nonrelativistic. Rather, the changes in spin coupling within the three electron system are inferred from the antisymmetry that is imposed on the wave function.

To illustrate how this kind of spin dynamics can manifest itself, we consider a simple thought experiment of sequential double photoionization of a spin-polarized three-electron system (such as atomic Li). An incoming high-energy photon can eject a $1s$ electron from the spin-polarized Li $1s^2 2s$ ground state. The resulting $1s2s$ state will be in a superposition of $1s2s$ ^1S and $1s2s$ ^3S. The $m_S = \pm 1$ components of this state can only be formed by the $1s2s$ ^3S state. However, the $m_S = 0$ component of this state created by photoionization consists of a coherent superposition of the ^1S and ^3S states. This superposition will now change over time between $|1s\uparrow 2s\downarrow\rangle$ and $|1s\downarrow 2s\uparrow\rangle$, due to the energy gap between the ^1S and ^3S states. Subsequent photoionization of the $2s$ electron by a short time-delayed pulse will then result in an observable time variation in the spin polarization of the ejected electron, signifying spin dynamics.

The RMT approach offers the capability to investigate such spin dynamics effects in an *ab initio* manner. This is demonstrated in Fig. 5, which shows the fraction of the three-electron wave function in which the innermost two electrons are coupled to triplet spin symmetry as a function of time for different electron-impact energies. Before the collision occurs, the innermost electrons are coupled to a singlet as the He atom is in the initial $1s^2$ ground state. During the collision, the incoming electron partially penetrates the ground state atom, becoming one of the innermost electrons. The coupling between impact electron and the other inner electron is partially described by a triplet coupling, causing the triplet spin fraction of the inner electrons to increase. After the collision, there is a notable probability for the impact electron to leave the atom, causing the original atomic electrons to return to being the inner electrons. This explains the later increase in singlet coupling.

Figure 5 suggests that, for our particular choice of initial wave packet, the main spin dynamics in this scattering process

occurs on a time scale that is dependent on the impact energy. We note that access to the full time-dependent wave function enables the use of different recoupling schemes, so it is possible to investigate the full range of dynamics in spin coupling between electrons. This may be of particular interest when more complex atoms with different residual-ion states, e.g., Ne^{2+}, are investigated.

IV. CONCLUSION

In summary, the RMT approach has been successfully applied to study dynamics on the attosecond time scale for three-electron systems from first principles. We have demonstrated that the RMT approach can reliably describe impact ionization processes involving double continua associated with different ionization thresholds. This includes processes where the incoming electron excites a superposition of doubly excited states, which leads to ultrafast dynamics in the subsequent autoionization. The autoionization rates in region (II) are in excellent agreement with benchmark calculations. With RMT, it is possible to extract both spin and spatial dynamics from a single calculation. The RMT codes hence provide a foundation for the investigation of intense-field multiple-ionization processes in three-electron systems as a stepping stone for our long-term aim to study such processes in general atoms.

ACKNOWLEDGMENTS

This research was sponsored by the Engineering and Physical Sciences Research Council (UK) under Grant Reference No. G/055416/1. This work also used the ARCHER UK National Supercomputing service (http://www.archer.ac.uk). We thank Dr. P. L. Bartlett and Prof. A. T. Stelbovics for providing PECS data. We additionally thank Dr. J. S. Parker for valuable discussions. Data from Figs. 1 to 5 can be accessed via http://pure.qub.ac.uk/portal/en/datasets/search.html.

[1] G. Sansone, F. Kelkensberg, J. F. Perez-Torres, F. Morales, M. F. Kling, W. Siu, O. Ghafur, P. Johnsson, M. Swoboda, E. Benedetti, F. Ferrari, F. Lepine, J. L. Sanz-Vicario, S. Zherebtsov, I. Znakovskaya, A. L'Huillier, M. Y. Ivanov, M. Nisoli, F. Martin, and M. J. J. Vrakking, Nature **465**, 763 (2010).

[2] M. Schultze, E. M. Bothschafter, A. Sommer, S. Holzner, W. Schweinberger, M. Fiess, M. Hofstetter, R. Kienberger, V. Apalkov, V. S. Yakovlev, M. I. Stockman, and F. Krausz, Nature **493**, 75 (2013).

[3] A. Schiffrin, T. Paasch-Colberg, N. Karpowicz, V. Apalkov, D. Gerster, S. Muhlbrandt, M. Korbman, J. Reichert, M. Schultze, S. Holzner, J. V. Barth, R. Kienberger, R. Ernstorfer, V. S. Yakovlev, M. I. Stockman, and F. Krausz, Nature **493**, 70 (2013).

[4] T. Popmintchev, M.-C. Chen, D. Popmintchev, P. Arpin, S. Brown, S. Ališauskas, G. Andriukaitis, T. Balčiunas, O. D. Mücke, A. Pugzlys, A. Baltuška, B. Shim, S. E. Schrauth, A. Gaeta, C. Hernández-García, L. Plaja, A. Becker, A. Jaron-Becker, M. M. Murnane, and H. C. Kapteyn, Science **336**, 1287 (2012).

[5] A. Temkin, Phys. Rev. **126**, 130 (1962).

[6] R. Poet, J. Phys. B **11**, 3081 (1978).

[7] P. L. Bartlett and A. T. Stelbovics, Phys. Rev. A **81**, 022715 (2010).

[8] P. L. Bartlett and A. T. Stelbovics, Phys. Rev. A **81**, 022716 (2010).

[9] M. S. Pindzola, D. Mitnik, and F. Robicheaux, Phys. Rev. A **59**, 4390 (1999).

[10] D. V. Fursa and I. Bray, Phys. Rev. A **52**, 1279 (1995).

[11] C. Plottke, I. Bray, D. V. Fursa, and A. T. Stelbovics, Phys. Rev. A **65**, 032701 (2002).

[12] C. Plottke, P. Nicol, I. Bray, D. V. Fursa, and A. T. Stelbovics, J. Phys. B **37**, 3711 (2004).

[13] D. A. Horner, C. W. McCurdy, and T. N. Rescigno, Phys. Rev. A **71**, 010701 (2005).

[14] C. Ruiz, L. Plaja, and L. Roso, Phys. Rev. Lett. **94**, 063002 (2005).

[15] M. A. Lysaght, L. R. Moore, L. A. A. Nikolopoulos, J. S. Parker, H. W. van der Hart, and K. T. Taylor, J. Phys. Conf. Ser. **388**, 012027 (2012).

[16] L. A. A. Nikolopoulos, J. S. Parker, and K. T. Taylor, Phys. Rev. A **78**, 063420 (2008).

[17] O. Hassouneh, A. C. Brown, and H. W. van der Hart, Phys. Rev. A **90**, 043418 (2014).

[18] T. Ding, C. Ott, A. Kaldun, A. Blättermann, K. Meyer, V. Stooss, M. Rebholz, P. Birk, M. Hartmann, A. Brown, H. van der Hart, and T. Pfeifer, Opt. Lett. **41**, 709 (2016).

[19] J. Wragg, J. S. Parker, and H. W. van der Hart, Phys. Rev. A **92**, 022504 (2015).

[20] P. Burke, *R-Matrix Theory of Atomic Collisions: Application to Atomic, Molecular and Optical Processes*, Springer Series on Atomic, Optical, and Plasma Physics (Springer, Berlin, 2011).

[21] D. R. Schultz, C. Bottcher, D. H. Madison, J. L. Peacher, G. Buffington, M. S. Pindzola, T. W. Gorczyca, P. Gavras, and D. C. Griffin, Phys. Rev. A **50**, 1348 (1994).

[22] D. M. Mitnik, Phys. Rev. A **70**, 022703 (2004).

[23] S. X. Hu and L. A. Collins, Phys. Rev. A **71**, 062707 (2005).